Available online at www.sciencedirect.com
SCIENCE DIRECT®
Journal of Nuclear Materials 346 (2005) 120–130
journal of nuclear materials
www.elsevier.com/locate/jnucmat

# Effect of microstructural evolution on in-reactor creep of Zr–2.5Nb tubes

YoungSuk Kim *, KyungSoo Im, YongMoo Cheong, SangBok Ahn

*Korea Atomic Energy Research Institute, Zirconium Group, P.O. Box 105, Yusong, Daejon 305-353, Republic of Korea*

Received 22 July 2004; accepted 4 June 2005

**Abstract**

Dislocation density, decomposition of the β-Zr phase and diametral creep were examined as a function of the location of the Zr–2.5Nb tube irradiated in the Wolsong Unit 1 for 9.3 effective full power years (EFPYs). The maximum a-dislocation density occurred at the inlet part of the irradiated Zr–2.5Nb tube exposed to the lowest temperature while the outlet part of the tube exposed to the higher temperature had the higher extent of decomposition of the β-Zr phase and the maximum diametral creep. Thus, it is concluded that in-reactor creep of the Zr–2.5Nb tube is not related to the dislocation density but governed by the Nb concentration of the α-Zr grains caused by thermal decomposition of the β-Zr phase. Supplementary creep tests on the Zr–2.5Nb sheets with different Nb contents in the β-Zr phase provide supportive evidence to this conclusion. The acceleration of the in-reactor creep of the Zr–2.5Nb tubes is suggested after a long-term operation.


*PACS:* 61.80.Hg

## 1. Introduction

When Zr–2.5Nb pressure tubes are operated in reactors, their microstructures evolve with neutron irradiation. Thus, it is very important to understand how their microstructures evolve with operational conditions such as fast neutron fluences and temperatures and what effects they have on the long-term degradation of pressure tubes. By investigating the effect of the microstructural evolution of Zr–2.5Nb tubes on corrosion, Urbanic reported that the β-Nb particles precipitated in the α-Zr grains is a governing factor to the lower corrosion of Zr–2.5Nb tubes under neutron irradiation [1]. However, no study has been undertaken so far on the effect of microstructural evolution on the in-reactor creep of Zr–2.5Nb tubes. Recently, Griffiths just reported that a big scatter in the creep rates of Zr–2.5Nb pressure tubes is largely due to variations in grain size, texture and oxygen content [2]. Though recognizing that the pressure tubes have their microstructures evolving during operation in reactors [3], he did not consider its effect on their creep and resulting scatter in the creep rates [2]. There are two factors to cause a microstructural change in the Zr–2.5Nb tubes: one is the fast neutron fluence ($E > 1$ MeV) and the other is temperature. The highest

* Corresponding author. Tel.: +82 42 868 2359; fax: +82 42 868 8346.
*E-mail address:* yskim1@kaeri.re.kr (Y.S. Kim).

0022-3115/$ - see front matter © 2005 Elsevier B.V. All rights reserved.
doi:10.1016/j.jnucmat.2005.06.004

fluence corresponds to the middle part of the tube due to a cosine shape of neutron flux while the highest temperature to the top part of the tube [4]. Thus, depending on the location of the tubes from the inlet part, the tubes would have different microstructural evolution and hence the creep. The objective of this study is to investigate microstructural changes with a distance from the inlet of the Zr–2.5Nb tube irradiated in the Wolsong Unit 1 for 9.3 EFPYs, or effective full power years, and their effect on the creep of the irradiated Zr–2.5Nb tubes. The irradiated tube was subjected to the maximum fluence of $8.9 \times 10^{25}$ n/m$^2$ at the middle part. To indirectly evaluate the effect of microstructural evolution on the creep of Zr–2.5Nb tubes, the creep behavior of Zr–2.5Nb sheets was investigated with the β-phase containing different Nb content.

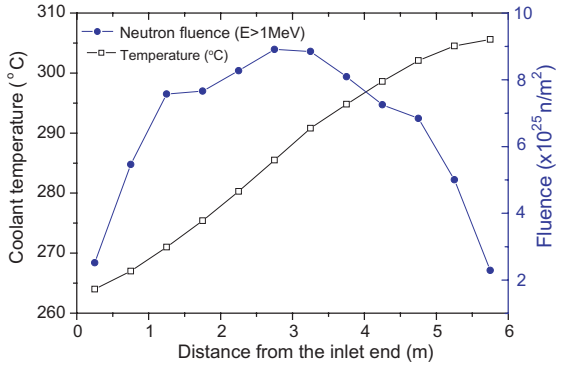


Fig. 1. Distribution of averaged coolant temperature and neutron fluence ($E > 1$ MeV) with a distance from the inlet of the Zr–2.5Nb tube.

## 2. Experimental procedures

### 2.1. Material

The examined Zr–2.5Nb had been operated in the M-11 channel of the Wolsong Unit 1 for 9.3 effective full power years [5]. A tube ring of about 170 mm long was taken from the inlet, the middle and the outlet of the tubes, respectively. The average temperature and neutron fluence to which each tube ring had been exposed ranged from 275.4 to 302.1 °C and from $6.84 \times 10^{25}$ to $8.9 \times 10^{25}$ n/m$^2$ ($E > 1$ MeV) as shown in Table 1 and Fig. 1. To simulate the microstructural evolution of Zr–2.5Nb tubes in reactors, Zr–2.5Nb sheets were made by four different manufacturing procedures as shown in Table 2. The energy dispersive X-ray analyses (EDX) were conducted on the carbon replicas with β-Zr particles extracted from the Zr–2.5Nb sheets. The Nb content determined ranged from 49 wt% to 82 wt%. depending on the manufacturing procedures (Table 3). Creep tests were conducted at 623–673 K under stress of 120 MPa on the specimens of 25 mm in gauge length, taken from the direction parallel to the rolling direction.

### 2.2. Determination of dislocation density and the Nb content in the β-Zr grains

Thin foils of 3 mm in diameter and 0.1 mm thick were cut out of the radial–circumferential plane of the irradiated tube to facilitate an analysis of c-type dislocations where there is a predominance of basal planes parallel to the electron beam. It should be noted that the examined Zr–2.5Nb tube has a strong circumferential texture with a high fraction of (0 0 0 1) basal planes in the circumferential direction [6]. Thin foils were electropolished in a solution of 10% perchloric acid and 90% ethanol at about −35 °C at the 20 voltages using a Tenupol-3 twin jet apparatus. TEM analyses were conducted using a Jeol-2000 FX (200 KeV) electron microscope equipped with a $LaB_6$ filament. The microstructural evolution such as dislocation loops and lines, precipitates and so on was investigated with bright and dark field imaging and selected area diffraction. Dislocation density was determined by a line intercept method where the number of the intersections between concentric circles or straight lines and dislocations were counted:

$$\rho = \frac{2N}{Lt},$$

where $N$ is the number of the intersections of dislocations, $L$ is a secant circle length or line length and $t$ is a foil thickness. The foil thickness was determined by measuring a change in the width of the projected grain boundary or sub-grain boundary with tilting, ranging from 500 to 2000 A [7].

The Nb content in the β-Zr phase was determined in two ways: one is the selected diffraction patterns (SADPs) on the thin foils and the other is the EDX on

Table 1
Operating conditions of the examined tube

| Location | Distance from the inlet (cm) | Coolant temperature (°C) | Fast neutron fluence ($E > 1$ MeV) (×10$^{25}$ n/m$^2$) |
|---|---|---|---|
| Inlet | 173–190 | 275.4 | 7.66 |
| Middle | 266–283 | 285.5 | 8.91 |
| Outlet | 456–483 | 302.1 | 6.84 |

Table 2
Manufacturing processes to make Zr–2.5Nb sheets with different Nb contents in the β-Zr phase

| Process | P1 | P2 | P3 | P4 |
|---|---|---|---|---|
| Procedures | Ingot – homogenization treatment at 1323 K – hot rolling at 1132 K – final cold rolling (30%) – final anneal at 723 K for 24 h | Ingot – homogenization treatment at 1323 K – hot rolling at 1132 K – cold rolling – intermediate anneal at 865 K – cold rolling – intermediate anneal at 865 K – homogenization 1132 K and water quench – final cold rolling (30%) – final anneal at 723 K for 24 h | Ingot – homogenization treatment at 1323 K – hot rolling at 843 K – intermediate anneal at 865 K – cold rolling – intermediate anneal at 865 K – cold rolling – intermediate anneal at 865 K – final cold rolling (50%) – final anneal at 723 K for 24 h | Ingot – homogenization treatment at 1323 K – hot rolling at 973 K – intermediate anneal at 953 K – cold rolling – intermediate anneal at 865 K – cold rolling – intermediate anneal at 865 K – final cold rolling (50%) – final anneal at 723 K for 24 h |

the carbon replicas with extracted β-Zr particles as shown in Fig. 2. More details of the procedures to determine the Nb content in the β-Zr phase were reported elsewhere [7].

## 3. Results and discussion

### 3.1. Dislocation density distribution along the Zr–2.5Nb tube

Fig. 3 shows the microstructures of the irradiated Zr–2.5Nb pressure tube at the inlet, the middle and the outlet positions along with that of the as-fabricated Zr–2.5Nb. Here, the as-fabricated Zr–2.5Nb tube represents the back end off-cut of the examined tube before irradiation. The irradiated Zr–2.5Nb tube had many shaded and elongated α-Zr grains while the as-fabricated Zr–2.5 N tube did very clean and elongated α-Zr grains. Higher magnification of the microstructures as shown in Fig. 4 revealed that the shaded α-Zr grains are attributed to a lot of small loops of a-type dislocation with a maximum diameter of 5 to 10 nm, which did not appear in the as-fabricated Zr–2.5Nb tube. The results shown in Figs. 3 and 4 qualitatively demonstrate that the neutron irradiation yields tangled networks of small a-type dislocation loops, increasing the density of a-type dislocation but does not change the shape of α-Zr grains. Fig. 5 shows the c-type dislocations of the as-fabricated and irradiated Zr–2.5Nb pressure tubes. They appeared as straight lines when imaged with a 0002 diffraction vector in a prism foil. No loops of c-type dislocations were observed. It appears that the density of c-type dislocations looks very low and has many similarities between the as-fabricated and irradiated Zr–2.5Nb tubes, and insensitive to the location of the irradiated tube. Table 4 shows the density of a-type and c-type dislocations which were determined respectively at the inlet, middle, outlet locations of the irradiated Zr–2.5Nb tube and from the as-fabricated Zr–2.5Nb tube using a line intercept method. The a-type dislocation density of the irradiated Zr–2.5Nb tube was the highest ($7.5 \times 10^{14}/m^2$) at the inlet location with lower temperature of 275.4 °C and the lowest ($5.2 \times 10^{14}/m^2$) at the outlet location exposed to higher temperature of 302 °C, both of which were higher than the a-type dislocation density of the as-fabricated Zr–2.5Nb tube ($4.0 \times 10^{14}/m^2$). To the contrast, the density of c-type dislocations was all the same independent of the location of the irradiated Zr–2.5Nb tube, which was the same as that of the as-fabricated tube as shown in Table 4. Thus, it is concluded that the neutron irradiation with a fluence of up to $8.9 \times 10^{25}$ n/m$^2$ ($E > 1$ MeV) increases a-type dislocation density very effectively at the inlet location of the Zr–2.5Nb tube exposed to the lowest temperature during its operation in the reactor compared with that of the

Table 3
Microchemical composition of the β-Zr phase determined by EDX on the extracted particle from the Zr–2.5Nb sheets made with four different manufacturing processes

| Process | P1 | P2 | P3 | P4 |
|---|---|---|---|---|
| Nb content in the β-Zr phase (at.%) | 49 | 62 | 82 | 81 |

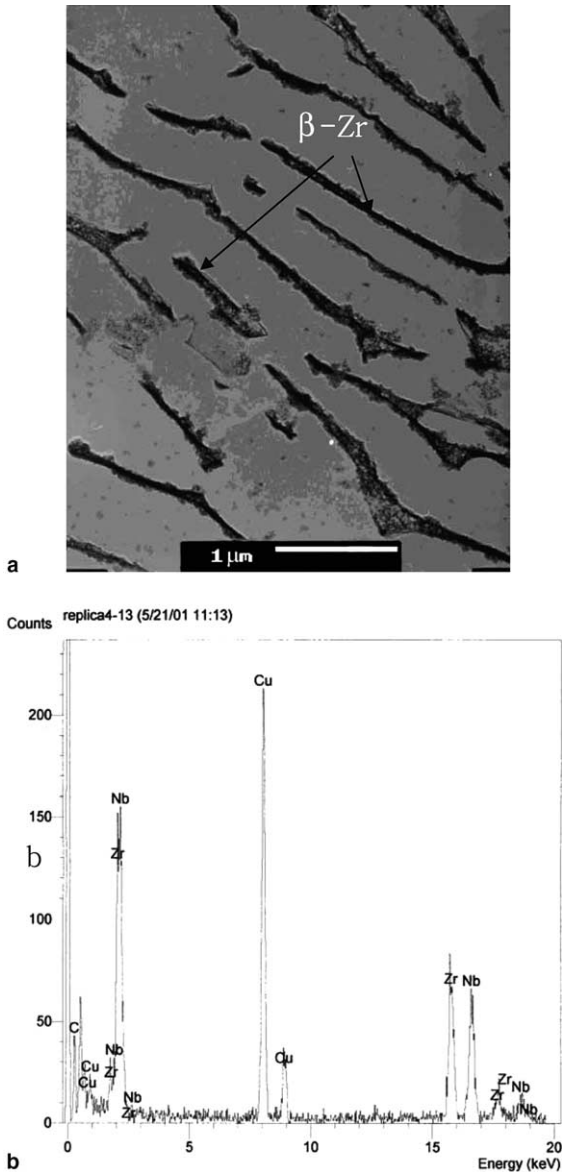


Fig. 2. (a) Micrograph of the β-Zr phase extracted from Zr–2.5Nb pressure tube by a carbon replica film and (b) the EDX analysis of the extracted β-Zr phase.

as-fabricated Zr–2.5Nb tube but little changes the concentration of c-type dislocation. This is probably due to an easier slip of the dislocations on the prism plane than on the basal plane when the Zr–2.5Nb tube is subjected to the circumferential stress of around 150 MPa under the neutron irradiation of $8.9 \times 10^{25}$ n/m$^2$ ($E > 1$ MeV).

### 3.2. Phase change along the Zr–2.5Nb tube

One of the main features of the irradiated Zr–2.5Nb pressure tube is the precipitation of small needle-like particles in the α-Zr grains as shown in Fig. 6. These particles look like β-Nb particles appearing after either the irradiation of neutron, proton or electron or aging [8–11] even though they are too small to determine their composition by the EDX. These needle-like particles appeared on the irradiated Zr–2.5Nb tube independent of the location, which could not be observed in the as-fabricated tube (Fig. 6). The average size of the precipitates ranged from 4 nm at the inlet to 4.7 nm at the outlet (Fig. 6(c)), likely suggesting some growth of the precipitates occurring at the outlet part of the tube exposed to higher temperature (Table 4).

A phase change of the β-Zr grains was also investigated on the irradiated Zr–2.5Nb tube. An X-ray microanalyzer was applied on the thin foils and the carbon replicas with extracted particles to determine the Nb content of the β-Zr grains. The surprising thing is that the Nb content and its distribution along the irradiated tube were not consistent between analytical methods: X-ray diffraction patterns on thin foils or EDX on extracted particles on carbon replicas. The former showed a concavely parabolic distribution of the Nb content along the tube with a minimum Nb content at the middle part as shown in Fig. 7. These results seems to agree with Griffiths' result determined using an X-ray method from the Zr–2.5Nb tubes irradiated for 2 to 12 years at temperatures ranging from 247 to 297 °C [3,12]. However, the latter yielded a linear increase in the Nb content of the β-Zr phase along with a distance from the inlet of the irradiated tube as shown in Fig. 7, which is different from Griffiths' result. Considering that the carbon replica specimen can yield more accurate analysis of the Nb content in the β-Zr grains, we come to a conclusion that the outlet part of the Wolsong 1 tube exposed to a higher temperature has an increased Nb content in the β-Zr grains due to a faster thermal decomposition of the β-Zr phase, and the inlet part exposed to comparatively lower temperatures has the decreased Nb content in the β-Zr grains below that in the as-fabricated tube

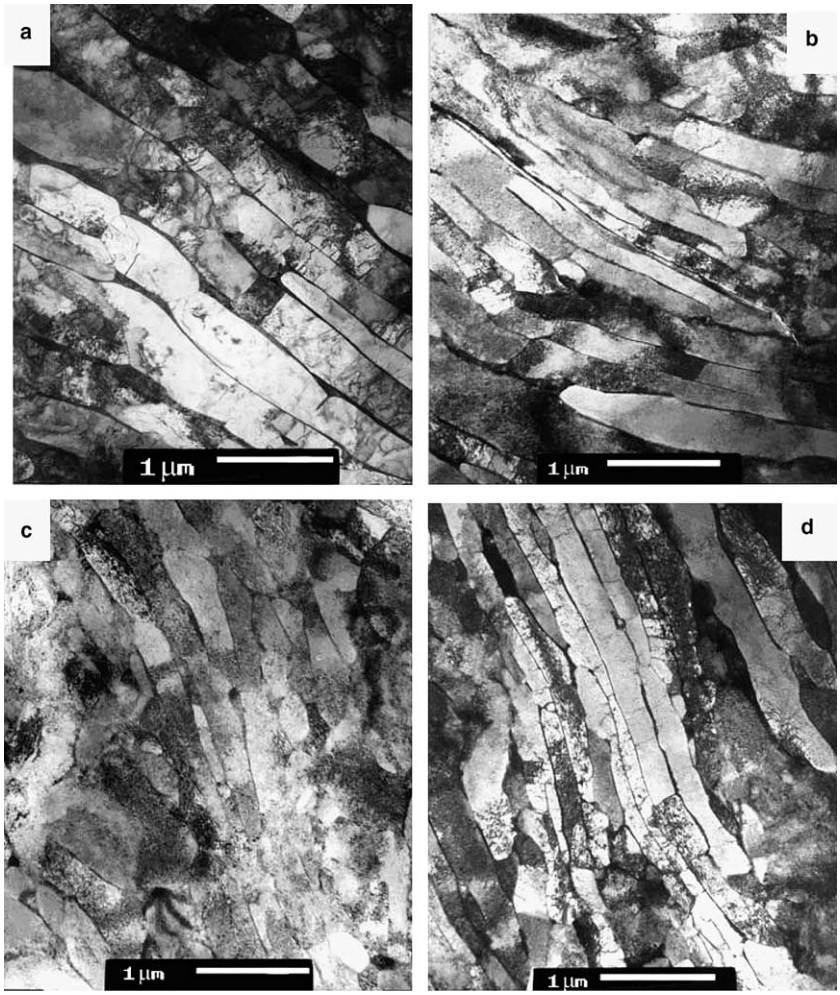


Fig. 3. Microstructures of (a) the as-fabricated Zr–2.5Nb tube, and (b) the inlet part, (c) the middle part and (d) the outlet part of the irradiated Zr–2.5Nb tube.

due to the neutron irradiation. In other words, the thermal diffusion effect facilitates the Nb supersaturated in the α-Zr grains to move to the β-Zr, transforming it to the β-Nb (or leading to the decomposition of the β-Zr phase) while the neutron irradiation effect causes the Nb in the β-Zr grains to dissolve into the α-Zr grains as a result of radiation enhanced dissolution [13]. Thus, it suggests that the Nb continuously moves back and forth between the α-Zr and the β-Zr grains depending upon the operating conditions of the Zr–2.5Nb tubes in the reactor: when the thermal diffusion becomes dominant, the decomposition of the β-Zr grains results from diffusion of the Nb from the α-Zr to the β-Zr but the dissolution of the β-Zr by neutron irradiation becomes dominant at a lower temperature, letting the Nb move back from the β-Zr to the α-Zr. Therefore, the enhanced decomposition of the Wolsong 1 tube at the upper part as shown in Fig. 7 seems to be due to the higher operating temperatures of the Wolsong 1 tube ranging from 264 to 306 °C compared to those of the tubes (247–297 °C [12]) used for Griffiths' result. The decrease of the Nb content in the β-Zr grains by neutron irradiation was also reported by Urbanic [14] demonstrating that the radiation enhanced dissolution was more notable at the inlet location of the Zr–2.5Nb tubes.

### 3.3. Diametral in-reactor creep of the Zr–2.5Nb tube

Fig. 8 shows the inner tube diameter measured using CIGAR (channel inspection and gauging apparatus for reactors) equipment along the location of the Zr–2.5Nb after 9.3 EFPY-operation in the Wolsong Unit 1. The maximum creep corresponded to a distance of 4–5 m from the inlet part of the tube, corresponding to where the largest extent of thermal decomposition of

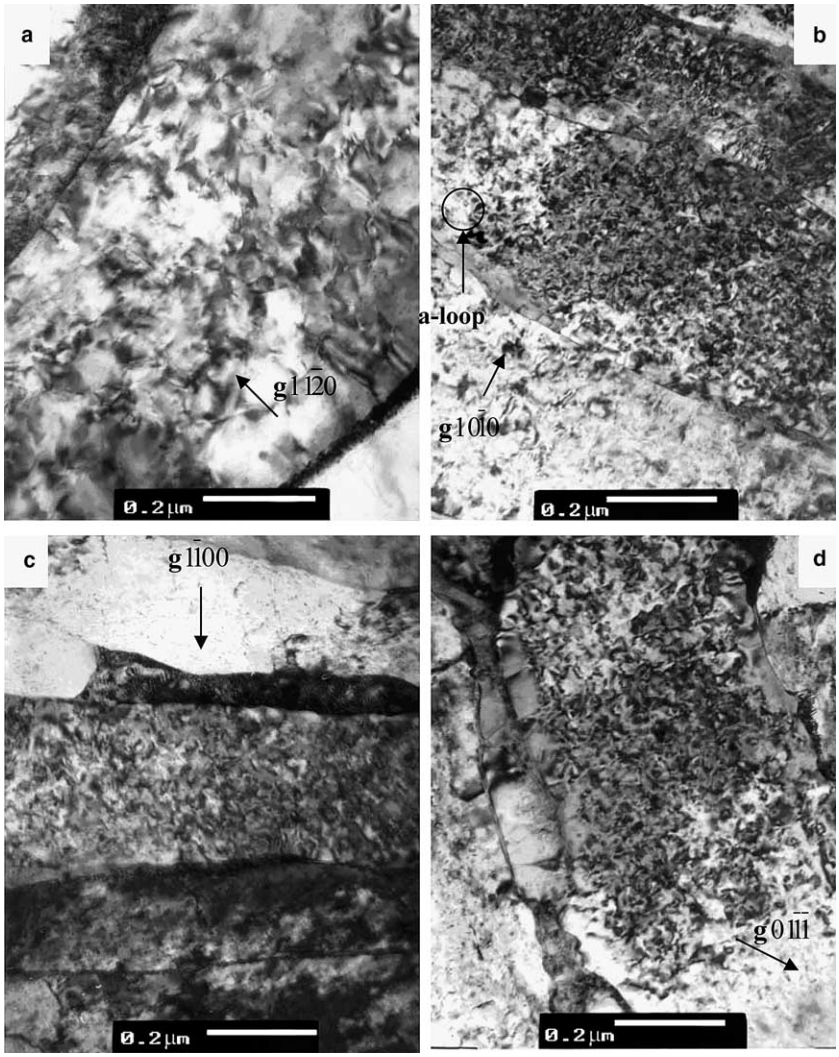


Fig. 4. Enlarged microstructures of α-Zr grains in (a) the as-fabricated Zr–2.5Nb tube and (b) the inlet part, (c) the middle part and (d) the outlet part of the irradiated Zr–2.5Nb tube.

the β-Zr grains has occurred. It is very surprising to note that the maximum creep does not correspond to the center position of the tube with the maximum fluence (or flux) as shown in Fig. 1. This explicitly indicates that the creep of the Zr–2.5Nb tube is not governed mainly by the neutron fluence but by something else. The increased Nb content in the β-Zr grains at the upper part of the tube as shown in Fig. 7 is accompanied by a decrease of the Nb concentration in the α-Zr grains due to the thermal diffusion, which seems to be responsible for a higher diametral creep in that region. In other words, the Nb concentration dissolved in the α-Zr grains determines the creep of the Zr–2.5Nb tubes due to the solution hardening effect: the lower the Nb concentration in the α-Zr grains becomes, the higher the creep of the irradiated Zr–2.5Nb tube. Considering the dislocation density distribution along the tube as shown in Table 4, the dislocation density likely has no effect on the diametral creep of the Zr–2.5Nb tube. In addition to that, the precipitation of β-Nb precipitates in the α-Zr grains may positively contribute to the enhancement of the creep due to a decrease of the dissolved Nb concentration in the α-Zr grains even though its effect is yet to be determined.

To correlate the Nb content in the β-Zr grains and the creep rate, the Zr–2.5Nb sheets were made with the Nb content in the β-Zr phase varying from 49 at.% to 82 at.% as shown in Table 2. Fig. 9 shows their microstructures made with four different manufacturing procedures. The Zr–2.5Nb sheet made with the procedure P1 had elongated α-Zr grains and β-Zr grains in between them, which is very similar to the microstructure of the

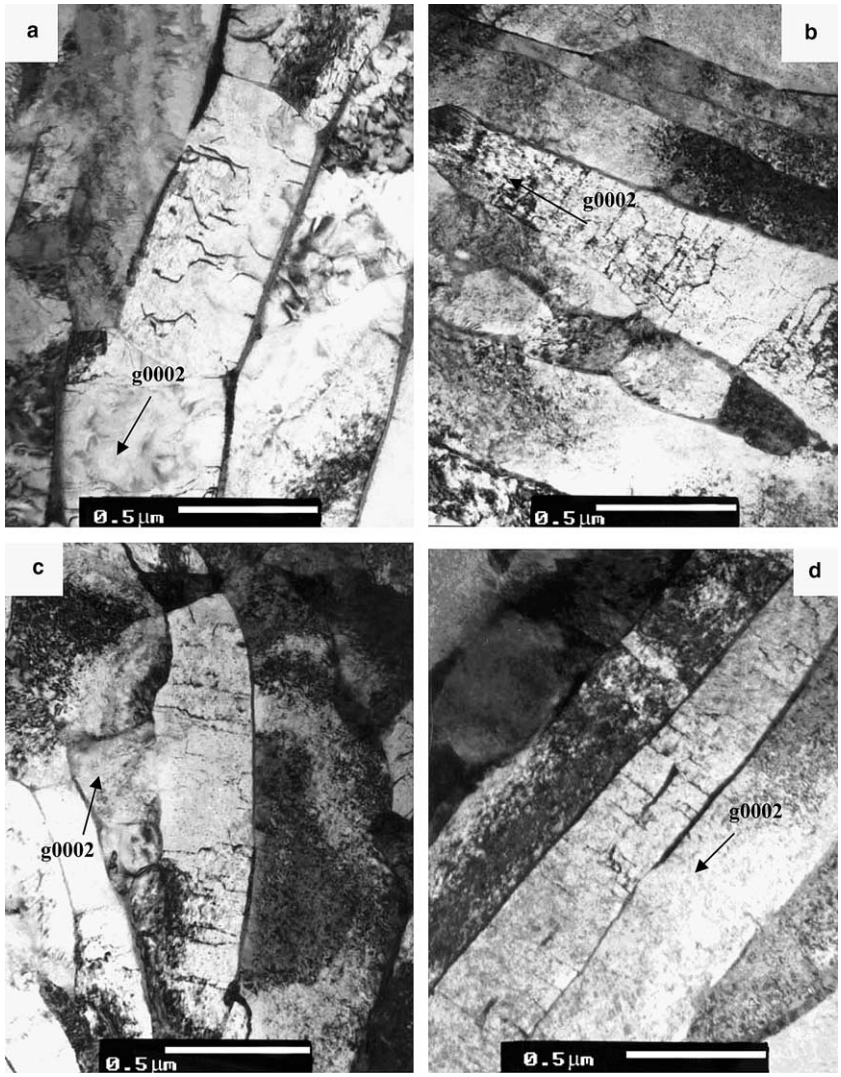


Fig. 5. c-Type dislocations observed in (a) the as-fabricated Zr–2.5Nb tube and (b) the inlet part, (c) the middle part and (d) the outlet part of the irradiated Zr–2.5Nb tube.

Table 4
Microstructural features of the irradiated Zr–2.5Nb tube with a distance from the inlet along with those of the as-fabricated Zr–2.5Nb tube

| Materials | a-Type dislocation ($\times 10^{14}$ m$^{-2}$) | c-Type dislocation ($\times 10^{14}$ m$^{-2}$) | β-Nb precipitates (nm) |
|---|---|---|---|
| As-fabricated Zr–2.5Nb tube | 4.0 | 0.97 | None |
| The irradiated Zr–2.5Nb tube | | | |
| 180 cm | 7.5 | 0.8 | 4.1 |
| 270 cm | 6.2 | 0.8 | 4.0 |
| 470 cm | 5.2 | 0.8 | 4.7 |

Zr–2.5Nb pressure tube, while the sheet with the procedure P2 had transformed α′-Zr grains of fine plate shape and larger prior α-Zr plates with partly decomposed β-Zr grains of spherical shape. These Zr–2.5Nb sheets made with the procedures P1 and P2 simulate the microstructures of the Zr–2.5Nb tube before irradiation. In

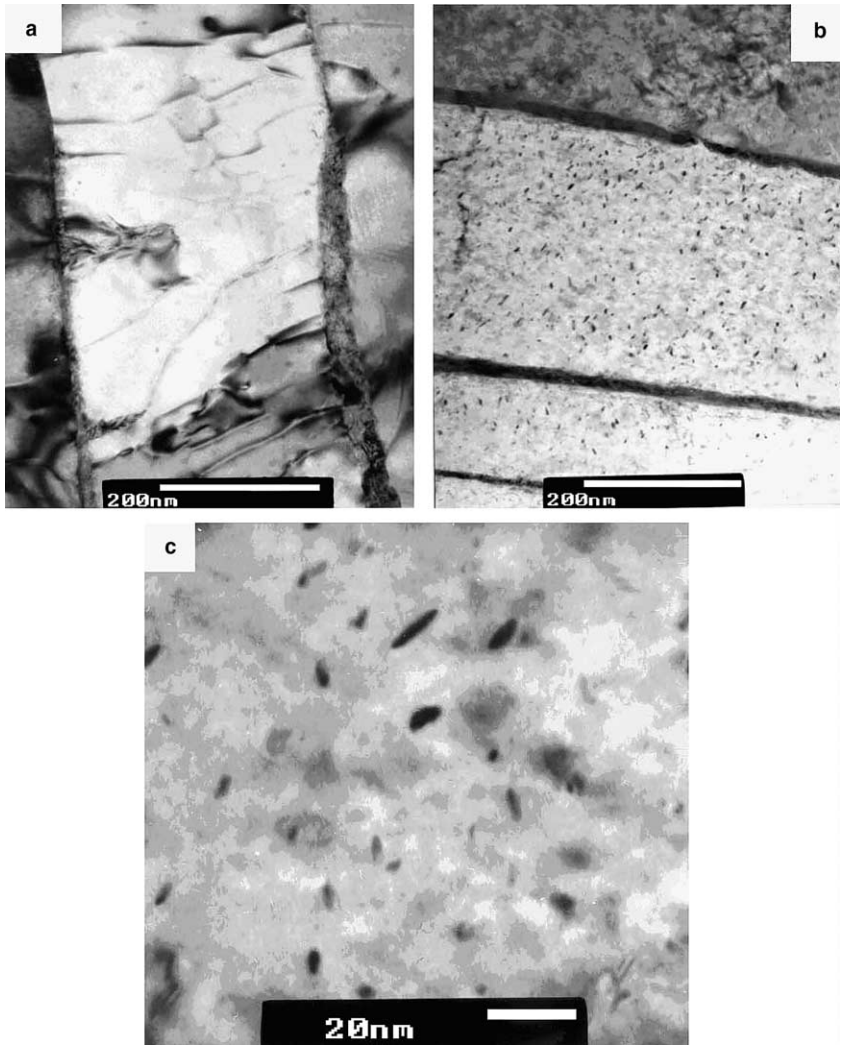


Fig. 6. β-Nb particles are observed not in (a) the as-fabricated Zr–2.5Nb tube but in (b) the irradiated Zr–2.5Nb tube. (c) is an enlarged photo of (b) showing the fine particles of a needle shape precipitated on the outlet part of the irradiated Zr–2.5Nb tube.

contrast, the P3 and P4 provided the Zr–2.5Nb sheets with the equilibrium microstructures of α-Zr grains and β-Nb grains except the formation of a few large recrystallized α-Zr grains in case of the P4. The Zr–2.5Nb sheets with the procedures P3 and P4 simulate the microstructures of the Zr–2.5Nb tube after a long-term irradiation. The creep tests were conducted at temperatures ranging from 350 to 400 °C under 120 MPa on the specimen whose axes are parallel to the rolling direction of these four sheets. The creep tests continued for up to 200 days enough to reach the steady creep rate. As shown in Fig. 10, the Zr–2.5Nb made with the P1 and P2 had lower creep rate or higher creep strength than the Zr–2.5Nb made with the P3 and P4. In other words, the Zr–2.5Nb alloy containing α-Zr grains and the β-Zr with larger Nb concentration had higher creep rate than that of the Zr–2.5Nb containing α-Zr grains and the β-Zr with lower Nb concentration. In short, the creep strength of the Zr–2.5Nb sheet strongly depends on the extent of decomposition in the β-Zr phase accompanied by a decrease of the Nb content in the α-Zr grains. Therefore, these supplementary results confirm that the phase decomposition accompanied in the Zr–2.5Nb tube contributes to enhancement of the diametral creep of the Zr–2.5Nb tubes. Since decomposition of the β-Zr phase accompanies the diffusion of Nb away from the α-Zr grains to the β-Zr grains, a governing factor for the creep of the Zr–2.5Nb seems to be the concentration of Nb in the α-Zr grains. In conclusion, the higher diametral creep at the upper region of the tube as shown in Fig. 8 must be attributed to the fast decomposition mainly by thermal effect, not by neutron

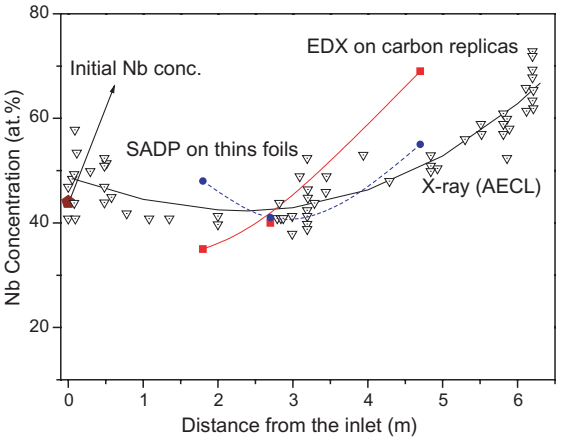


Fig. 7. Distribution of the Nb content in the β-Zr phase with a distance from the inlet of the Zr–2.5Nb tube irradiated in Wolsong Unit 1 for 9.3 EFPYs.

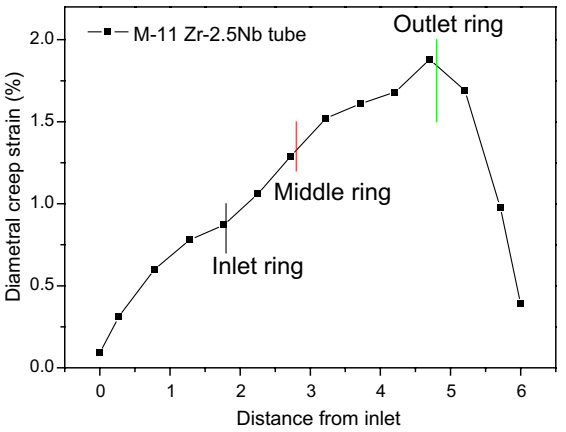


Fig. 8. Diametral creep strain of the M-11 Zr–2.5Nb tube with a distance from the inlet after the 9.3 effective full power year operating. Here, the inlet, middle and outlet rings shown in the plot indicate the position where each tube ring were taken from the M-11 tube.

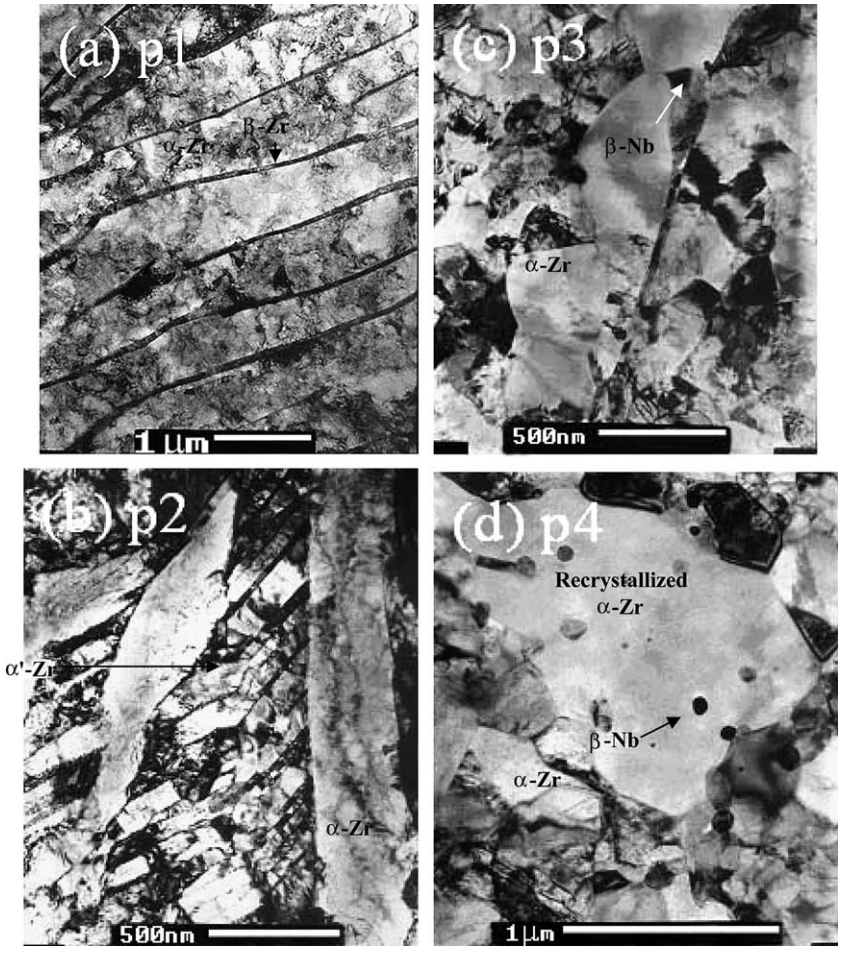


Fig. 9. Microstructures of the Zr–2.5Nb sheets made with four different manufacturing processes.

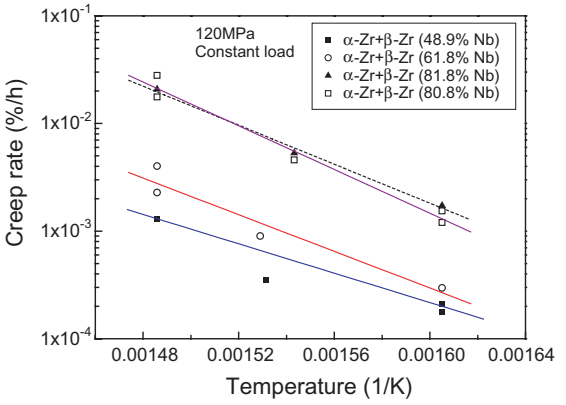


Fig. 10. Creep Rate of the Zr–2.5Nb sheets made with four different manufacturing processes under the applied stress of 120 MPa and temperatures of 350–400 °C.

irradiation. Since the decomposition of the β-Zr phases in the Zr–2.5Nb tubes would become larger with increasing operational time in reactors, the diametral creep rate is expected to become enhanced until the Zr–2.5Nb reaches the equilibrium microstructures. Since the microstructural evolution of Zr–2.5Nb tubes changes sensitively with the operating conditions such as coolant temperature and channel power, it seems to significantly contribute to a big scatter in the creep rate of Zr–2.5Nb tubes. Thus, the microstructural evolution should be considered in modeling an in-reactor creep of Zr–2.5Nb tubes in addition to manufacturing variables such as grains sizes, texture and oxygen content. When the Zr–2.5Nb tubes have their microstructure transformed fully to an equilibrium microstructure of α-Zr and β-Nb after a long-term operation in reactors, thus, they may have a non-linear creep rate deviating from a linear relationship after a long-term operation.

## 4. Conclusion

The irradiated Zr–2.5Nb tube in the Wolsong Unit 1 for 9.3 EFPYs had microstructural evolution: a change in the dislocation density and the Nb content in the β-Zr grains. The larger increase in the a-type dislocation density occurred at the inlet part of the irradiated Zr–2.5Nb subjected to the lowest operating temperatures. The outlet part with highest operating temperature had the largest extent of decomposition of the β-Zr grains accompanied by the depletion of the Nb from the α-Zr gains due to thermal diffusion while the inlet part had the decreased Nb content in the β-Zr grains due to radiation enhanced dissolution. It suggests that the Nb diffuses back and forth between the α-Zr and β-Zr grains in the Zr–2.5Nb tubes during their operation in the reactor due to a competition between thermal diffusion by temperature and radiation enhanced dissolution. Therefore, the higher in-reactor creep of the Zr–2.5Nb tubes at the upper region is concluded to be attributed to the decreased Nb content in the α-Zr grains arising from faster thermal decomposition at the outlet location subjected to a higher temperature, independent of the a-dislocation density. Supplementary creep tests demonstrate that with the lower Nb content in the α-Zr grains or with the higher Nb content in the β-Zr grains, the larger the creep rate of the Zr–2.5Nb sheets becomes, providing supportive evidence to the conclusion. Thus, the microstructural evolution should be considered one of the important variables in creating a scatter of in-reactor creep of Zr–2.5Nb tubes and seems to contribute to the acceleration of the creep of Zr–2.5Nb tubes with time.

## Acknowledgements

This work has been carried out as part of the Nuclear R&D program supported by Ministry of Science and Technology, Republic of Korea. One of the authors would like to express his sincere thanks to Dr Andrei Tshelishchev and Mr Seon Sik Kim for TEM works on the irradiated tube in hot cells.

## References

[1] V.F. Urbanic, M. Griffiths, in: Proceedings of the 12th Symposium on Zirconium in the Nuclear Industry, ASTM STP 1354, 2000, p. 641.
[2] M. Griffiths, W.G. Davies, A.R. Causey, G.D. Moan, R.A. Holt, S.A. Aldridge, in: Proceedings of the 13th Symposium on Zirconium in the Nuclear Industry, ASTM STP, 2002, to be published.
[3] M. Griffiths, J.F. Mecke, J.E. Winegar, in: Proceedings of the 11th Symposium on Zirconium in the Nuclear Industry, ASTM STP 1295, 1996, p. 580.
[4] Korea Electric Power Corporation, in: Final Safety Analysis Report for Wolsong Unit 1, Chapter 5, 1983.
[5] B.S. Han, Memo for Wolsong 1 Fuel Channels, Korea Electric Power Corporation, 1999.
[6] Y.S. Kim, S.S. Kim, Y.M. Cheong, K.S. Im, J. Nucl. Mater. 317 (2003) 117.
[7] Y.S. Kim, KAERI Report, KAERI/TR-1490/2000, Korea Atomic Energy Research Institute, 2000.
[8] C.E. Coleman, R.W. Gilbert, G.J.C. Carpenter, G.C. Weatherly, in: J.R. Holland, L.K. Mansur, D.I. Potter (Eds.), Proceedings of Phase Stability during Irradiation, 1980, p. 587.
[9] C.D. Cann, C.B. So, R.C. Styles, C.E. Coleman, J. Nucl. Mater. 205 (1993) 267.
[10] O.T. Woo, G.M. McDougall , R.M. Hutcheon, V.F. Urbanic, M. Griffiths, C.E. Coleman, in: Proceedings of the 12th Symposium on Zirconium in the Nuclear Industry, ASTM STP 1354, 2000, p. 709.

[11] C.P. Luo, G.C. Weatherly, Metall. Trans. A 19 (1988) 1153.
[12] M. Griffiths, P.H. Davies, W.G. Davies, S. Sagat, in: Proceedings of the 13th Symposium on Zirconium in the Nuclear Industry, ASTM STP, 2002, to be published.
[13] R.S. Nelson, J.A. Hudson, D.J. Mazey, J. Nucl. Mater. 44 (1972) 318.
[14] V.F. Urbanic, M. Griffiths, in: Proceedings of the 12th Symposium on Zirconium in the Nuclear Industry, ASTM STP 1354, 2002, p. 641.